https://dx.doi.org/10.1016/j.compscitech.2022.109440

Harnessing impact-induced cracking via stiffness heterogeneity

Ji Lin[1,2,3], Yujie Xie[1], Manqi Li[2], Jin Qian[2], Haimin Yao[1,*]

[1]Department of Mechanical Engineering, The Hong Kong Polytechnic University, Hung Hom, Kowloon, Hong Kong SAR, China

[2]Department of Engineering Mechanics, Key Laboratory of Soft Machines and Smart Devices of Zhejiang Province, Zhejiang University, Hangzhou 310027, China

[3]Piezoelectric Device Laboratory, Faculty of Mechanical Engineering & Mechanics, Ningbo University, Ningbo 315211, China

[*]To whom correspondence should be addressed, E-Mail: mmhyao@polyu.edu.hk (H. Yao)

Abstract

Mechanical heterogeneity refers to the spatial inhomogeneity of the mechanical properties in materials, which is a common feature of composites consisting of multiple distinct phases. Generally, the effects of mechanical heterogeneity on the overall properties of the composites, such as stiffness and strength, are thought to follow the rule of mixture. Here, we investigate the cracking behavior of composite plates under impact and found that the rule of mixture may break down in describing the cracking resistance of composites with high stiffness heterogeneity. Our results show that the resistance of a composite plate, which consists of two phases of distinct stiffnesses, against dynamic cracking strongly depends on the hybridizing manner of the two phases. When the stiff phase is dispersed in the compliant matrix, the resulting composite plate exhibits superior cracking resistance compared to the monolithic plates made of either phase. In contrast, if the compliant phase is dispersed in the stiff matrix, the resulting composite plate displays reduced cracking resistance and thus higher absorption of the impact energy as compared to the monolithic controls. Our work provides an approach to harnessing the dynamic fracture by controlling the stiffness heterogeneity, which would be of great value to the design and fabrication of the protective armors and energy-absorbing shields.

Keywords: Mechanical heterogeneity, Ballistic cracking, Crack-inclusion interactions, Structure-property relationship, Protective armors

1. Introduction

The mechanical properties and behavior of solid materials are determined not only by their chemical compositions but also by the way of how these compositions are bonded together in space, namely the so-called structure. Revealing the structure-property relations and then applying them to direct the design and manufacturing of new materials is an everlasting topic in materials science and engineering. As a typical structural attribute, mechanical heterogeneity refers to the spatial variation and inhomogeneity of the mechanical properties (*e.g.*, elasticity and plasticity) in materials. It is commonly observed at multiple length scales in materials consisting of constituent phases with distinct properties such as engineering composites [1-4] and natural biological materials [5-9]. Mechanical heterogeneity has been shown to play an important role in determining the overall mechanical properties of the composite materials. Normally, materials with high heterogeneity are believed to have inferior mechanical properties in comparison to the homogeneous counterparts made of similar chemical compositions. This is because the mechanical mismatch between the distinct building phases, upon external loading, tends to cause stress concentration and strain localization near the phase interfaces. Nevertheless, sometimes heterogeneity was also found to benefit the mechanical properties of the materials. For example, the heterogeneous-structured metallic materials achieved superior mechanical properties that are not accessible to conventional homogeneous counterparts [10]; a “brick-and-mortar” structure with high heterogeneity could effectively suppress the crack-induced stress intensification and fortify the flaw tolerance of nacreous composites [11]; a 10-15% micro- and nanomechanical heterogeneity was proved an optimal scheme to promote the ductile behavior of bones in nano- and microscale [12]. Particularly, the heterogeneity of plasticity at nano length scale in bones was demonstrated to promote energy dissipation during plastic deformation [13]. Moreover, heterogeneity in yield strength was found to benefit the strength-ductility synergy in metals [14].

In addition to plasticity, heterogeneity in stiffness, which is characterized by the elastic modulus, was found to influence the fracture behavior of a material. Related studies can be traced back to the investigations of the effect of an interface between two dissimilar elastic materials on the propagation tendency of a crack. It is found that the interface between dissimilar materials may enlarge or suppress the SIF of a crack in the front of it, depending on the stiffness heterogeneity across the interface. When the crack is situated on the compliant side of the interface and heads to the stiff side, the interface would suppress the SIF at the crack tip; in contrast, if the crack is situated on the stiff side of the interface and heads to the compliant side, the interface would enlarge the SIF at the crack tip [15-17]. This conclusion still holds when a crack embedded in an infinite elastic medium approaches to a circular inclusion with distinct elastic modulus, which is a basic physical picture of fracture in composites with heterogeneous stiffness. Tamate [18] and Atkinson [19] analytically solved the SIF at the crack tips under the influence of inclusion with different moduli and distances away from the crack. For more complicated cases, such as a crack under mixed-mode loading [20], the influence of interfacial strength between the inclusion and matrix [21], finite element method (FEM) was adopted to evaluate the SIF of a stationary crack in the presence of an inclusion. With the aid of the extended finite element method (XFEM), Jiang et al. [22, 23] found a similar effect of inclusions on the SIF of a dynamic crack tip. Tran and Truong [24] improved the smoothness of the stress and strain fields for the crack growth problem in composite material by incorporating XFEM with a twice interpolation method. The effect of inclusion on the SIF of a dynamic crack has been experimentally verified by the photoelasticity technique [25]. As a special inclusion with zero stiffness, a hole was also found to attract a crack propagating nearby [26], which is qualitatively in accord with previous studies. Further extensions were made to the studies on the effects of the heterogeneous interface on crack deflection and kinking [27, 28] and out-of-plane excursions of cracks [29]. Utilizing stiffness heterogeneity, researchers have effectively enhanced the fracture toughness of composites [30-32].

Although the loading and the geometries of the models in the above works were simplified, the revealed phenomena implied that stiffness heterogeneity might have a similar effect on impact-induced cracking and therefore can be applied to harness impact fracture. To verify this hypothesis, in this work we firstly carry out a systematic computational study on the effects of stiffness heterogeneity on the cracking caused by impact. Our study starts from the effect of circular inclusions on the growing tendency of a pre-existing crack under a static load. Then, the discussion is extended to the dynamic cracking in inclusion-matrix composites caused by ballistic impact. Two types of composites with complementary hybridizing schemes are studied: stiff inclusions embedded in a compliant matrix (S@C) and compliant inclusions embedded in a stiff matrix (C@S). Parametric studies on the effects of inclusion size, stiffness, volume fraction, inter-inclusion spacing, and distribution pattern are carried out, followed by the experimental verification of the effect of stiffness heterogeneity on cracking resistance. Finally, the paper is concluded after discussing the synergetic effect of the S@C and C@S composites under ballistic impact. The results obtained in the present study are believed to serve as a general guide for the development of anti-impact materials and protective shields.

2. Interference of stiffness heterogeneity with SIF of a static crack

To quantify the effect of stiffness heterogeneity on the propagation tendency of a crack, an idealized finite element (FE) model is constructed (ABAQUS/Standard, Dassault Systèmes), in which a square plate (edge length: $2D$) with pre-existing cracks contains a circular inclusion of radius R at the center (see Fig. 1(a)). Periodic boundary conditions are applied on both lateral sides of the model. That is, the model depicts a representative volume element (RVE) of a periodic structure with a period of $2D$. The thickness and the period of the model are taken as 5 mm and 100 mm, respectively. The inclusion and the matrix are assumed perfectly bonded. Young's modulus and Poisson's ratio of the matrix are prescribed as $E_{\mathrm{M}} = 10$ GPa and $\nu_{\mathrm{M}} = 0.3$, respectively. Eight-node linear brick elements with reduced integration (C3D8R in ABAQUS) are employed except in the region around the crack tip, where six-node linear triangular prism elements are applied to improve the accuracy in describing the singular stress field with square-root singularity. A uniform tensile stress σ_0 is applied along the direction perpendicular to the surface of the pre-existing cracks. The SIF (K_{I}) is derived from $K_{\mathrm{I}} = \sqrt{JE_{\mathrm{M}}}$, where J is the calculated J-integral around the crack tip [33]. Due to the symmetry of the model, we do not distinguish the two cracks in the model when discussing the SIF in the following.

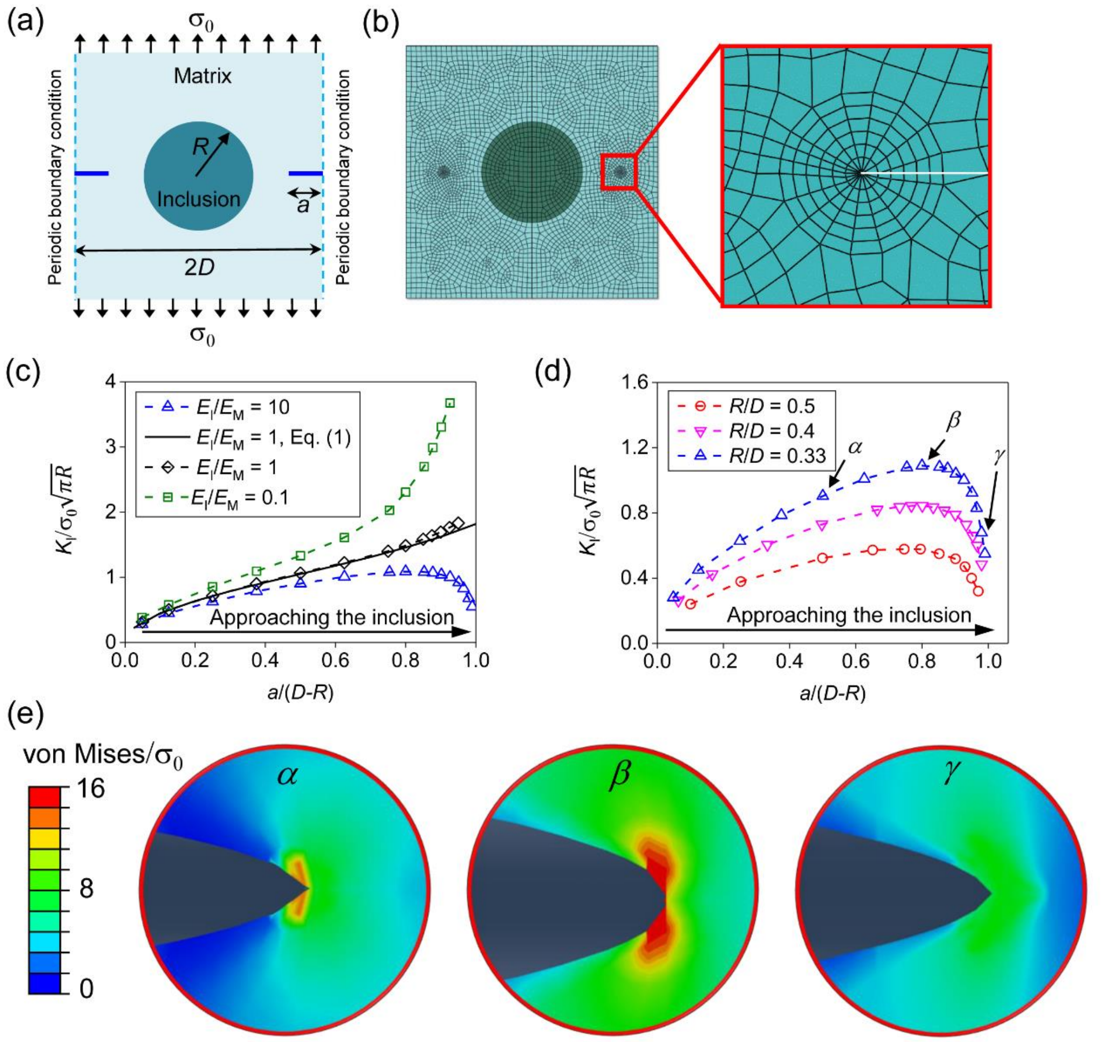

Figure 1. (a) The RVE model applied in finite element analysis; (b) Meshing of the model and enlarged view at the crick tip. Computed variation of the stress intensity factor (normalized) at the crack tip with the crack length (normalized) for inclusion-matrix composites with inclusions of (c) different stiffnesses, and (d) different sizes. The inclusion radius in (c) is taken as $R = 0.33D$ and the inclusion modulus in (d) is taken as $E_{\mathrm{I}} = 10\ E_{\mathrm{M}}$; (e) Snapshots of the von Mises stress field (normalized by the load σ_0) at three selected moments as indicated in (d). α: $a/(D-R) = 0.48$; β: $a/(D-R) = 0.75$; γ: $a/(D-R) = 0.98$.

Fig. 1(c) shows the calculated SIF as a function of crack length for three cases with inclusions of different stiffnesses: $E_{\mathrm{I}} = 10E_{\mathrm{M}}$, $E_{\mathrm{I}} = E_{\mathrm{M}}$ and $E_{\mathrm{I}} = 0.1E_{\mathrm{M}}$. For the homogeneous case with $E_{\mathrm{I}} = E_{\mathrm{M}}$, the analytical solution to the SIF exists and is given by [34]

$$K_{\mathrm{I}} = \sqrt{\frac{2D}{\pi a}\tan\frac{\pi a}{2D}}\,\sigma_0\sqrt{\pi a} \tag{1}$$

The consistency between such an analytical solution and our calculated results shown in Fig. 1(c) validates the calculated SIF in other cases. Comparison between the three cases shown in Fig. 1(c) confirms that stiffness heterogeneity affects the SIF, which determines the growing tendency of a crack. Particularly, stiff inclusion ($E_{\mathrm{I}} > E_{\mathrm{M}}$) suppresses the SIF and therefore resists the crack propagation, while compliant inclusion ($E_{\mathrm{I}} < E_{\mathrm{M}}$) enhances the SIF and therefore facilitates the crack propagation.

We further studied the size effect of the inclusions. Fig. 1(d) shows the variation of the calculated SIF with the crack length for cases with inclusions of different sizes and given modulus $E_{\mathrm{I}} = 10E_{\mathrm{M}}$. In these three cases, the SIF exhibits a similar variation trend with the increasing crack size. That is, it increases initially and then decreases with the increase of the crack size. Such variation of SIF can be further visualized from the stress (von Mises) field near the crack tip at three representative moments, as shown in Fig. 1(e). Comparison between these three studied cases indicates that larger inclusion imposes higher suppression on the SIF.

3. Effect of stiffness heterogeneity on ballistic cracking

3.1 Simulation of ballistic impact

To extend our study from static cracks to dynamic fracture, we simulated the ballistic impact process of a spherical projectile (radius: 2 mm) on composite plates (96 mm × 96 mm × 1 mm) composed of a stiff (S) phase and a compliant (C) phase, as shown in Fig. 2(a). The modulus of the stiff phase is taken as 10 times that of the compliant phase. To mask off the possible influence of the factors other than stiffness on the cracking behavior, the other properties of these two phases, such as density, Poisson’s ratio, fracture strength, and fracture energy are assumed the same. Both compliant phase and stiff phase are assumed as brittle materials with fracture energy $\Gamma = 10\,\mathrm{J\cdot m^{-2}}$, which is close to the fracture energy of glass (Fig. S1). As we are concerned about the cracking behavior in the composite plates, the material of the projectile is simply assumed as steel with linear elasticity. The detailed material properties of each phase and the projectile are summarized in Table 1. Two complementary hybridizing schemes for the composite plates are considered. One is to embed stiff inclusions into the compliant matrix (denoted as S@C), and the other is to embed compliant inclusions into the stiff matrix (denoted as C@S). For comparison, monolithic plates of the same dimensions composed of compliant phase or stiff phase only are applied as the control cases. Both plates and projectiles are modelled with four-node shell elements (S4R in ABAQUS) with a thickness of 1 mm. Simply-supported boundary conditions are applied on four vertexes of the plate. The initial velocity of the projectile is taken as $8\,\mathrm{m\cdot s^{-1}}$ perpendicularly towards the plate center. The friction coefficient between the projectile and plate is set as 0.2. The crack initiation and propagation in the plate upon the ballistic impact by the projectile are simulated by the element deletion technique (brittle cracking material model in ABAQUS/Explicit) [35], whereby an element is "deleted" by gradually reducing its stiffness to zero when its maximum principal stress reaches the prescribed fracture strength. During the crack opening, linear stress reduction is introduced to describe the stress variation of the element, which consumes the fracture energy of the material.

Table 1. Material properties adopted in FE simulations

Properties	Stiff Phase	Compliant Phase	Projectile
Density, ρ (g cm^{-3})	1.3	1.3	7.8
Young's modulus, E(GPa)	2	0.2	210
Poisson's ratio, ν	0.3	0.3	0.3
Fracture strength, σ_f(MPa)	2	2	-
Fracture energy, Γ (J m^{-2})	10	10	-

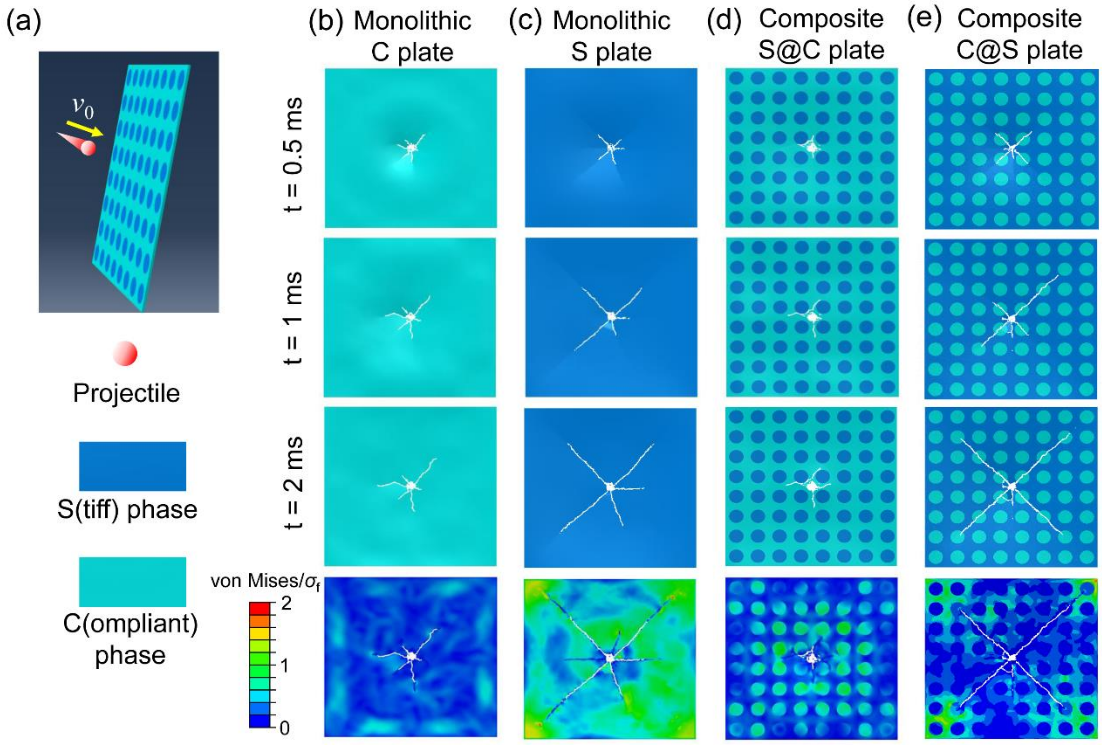

Figure 2. (a) Schematic showing the simulation model of a projectile perpendicularly impacting on a plate. (b-e) Snapshots of the calculated cracking process at time t = 0.5, 1, and 2 ms: (b) monolithic compliant plate, (c) monolithic stiff plate, (d) S@C composite plate, and (e) C@S composite plate. Von Mises stress distributions at t = 2 ms shown at the bottom row is normalized by the fracture strength (σ_{f}) of the materials. The radius of the inclusions in (d) and (e) is 4 mm, and the inter-inclusion spacing (center-to-center) is 12 mm.

3.2 Results and discussions

The snapshots of the cracking process of four plates upon ballistic impact are displayed in Fig. 2. For the two monolithic cases, it can be seen that cracks propagate faster and longer in the pure stiff plate (Fig. 2(c)) than in the pure compliant plate (Fig. 2(b)), although the fracture strength (σ_{f}) and fracture energy (Γ) of both materials are taken the same. This can be attributed to the lower toughness ($\frac{1}{2}\sigma_{\mathrm{f}}^2/E$) of the stiff material. If the fracture strength of the stiff material is increased to such a value that its toughness would be equal to that of the compliant material, both monolithic plates will exhibit similar cracking configurations under impact (see Fig. S2(a, b)). In the S@C composite plate (Fig. 2(d)), the ballistic cracks emitted from the impact point (compliant region) are deflected or blocked by the inclusions (stiff phase), and thereby crack propagation are constrained in a limited region; in contrast, in the C@S plate (Fig. 2(e)), the ballistic cracks initiating from the impact point (stiff region) penetrate and pass through the inclusions (compliant phase). Consequently, crack propagation is highly exacerbated in the C@S plate as compared to the S@C composite plate and two monolithic controls. Similar result is observed when the toughness ($\frac{1}{2}\sigma_{\mathrm{f}}^{2}/E$) of both phasic materials are taken as the same (see Fig. S2(c, d)). The contrast of different plates in resisting dynamic cracking shown in Fig. 2 (S@C > monolithic > C@S) also agrees with the effect of the heterogeneous interface on the SIF of a stationary crack as shown in Fig. 1. In both composite plates, the stress level in the compliant phase is lower than that in the stiff phase, implying that the ballistic cracks are prone to propagate into the regions with lower stress level.

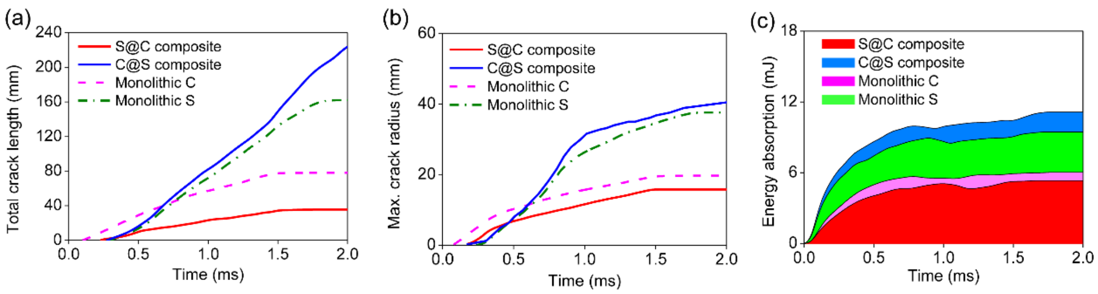

Figure 3. Calculated evolutions of (a) the total crack length, (b) the maximum crack radius, and (c) energy absorption with the time in the impact process. Here the total crack length and maximum crack radius are normalized by the radius of the projectile (R_{p}) and energy absorption is normalized by the initial kinetic energy of the projectile. This normalization scheme is applied throughout this paper.

To make a quantitative comparison between the results from different plates, we examined the total crack length and the maximum crack radius in the four simulated cases, as shown in Fig. 3(a) and Fig. 3(b) respectively. Here, the total crack length is calculated by summing up all the cracks developed in the plate, and the maximum crack radius is the length of the longest radial crack generated by the impact. Based on either the total crack length or the maximum crack radius as calculated, the cracking resistance of the four plates can be ranked in the following sequence: S@C composite > monolithic C > monolithic S > C@S composite. Moreover, we examined the energy absorption, which is defined as the loss of the kinetic energy of the projectile during impact (Fig. 3(c)). These four plates exhibit an opposite sequence in energy absorption: S@C composite < monolithic C < monolithic S < C@S composite. This makes sense because the absorbed energy is proportional to the total length of cracks generated in the plate given that the fracture energy (Γ) of both phases are presumably identical in our simulations.

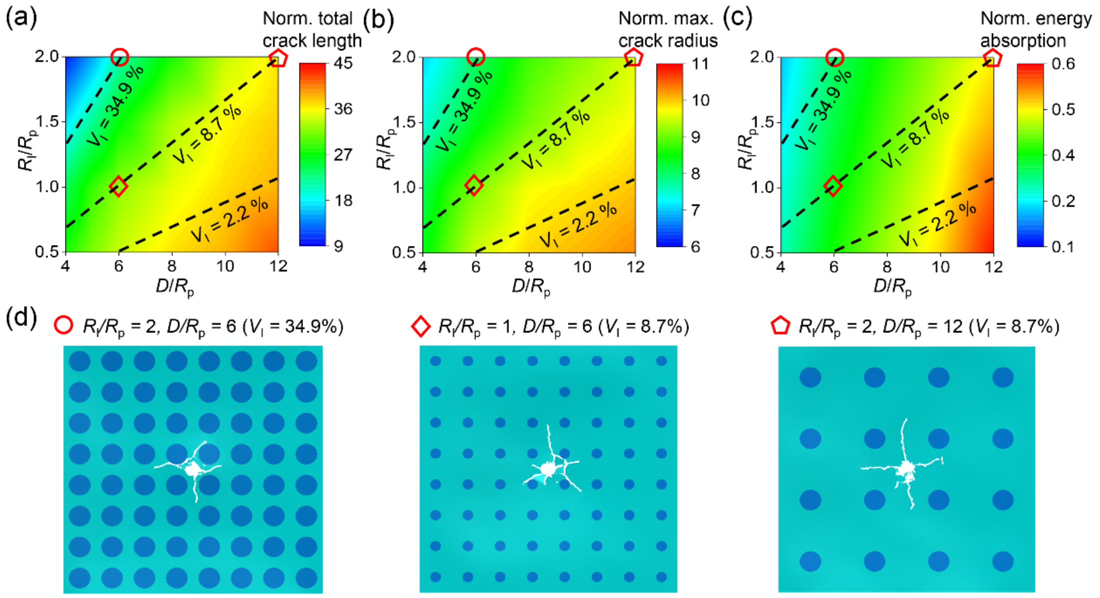

Figure 4. Contour maps of (a) total crack length, (b) maximum crack radius, and (c) energy absorption as functions of the normalized inclusion radius (R_I/R_p) and the normalized inter-inclusion spacing (D/R_p). Total crack length and maximum crack radius are normalized by the radius of the projectile (R_p) and the energy absorption is normalized by the initial kinetic energy of the projectile. (d) Post-impact configurations of three selected cases as marked by symbols of a circle, a diamond, and a pentagon in (a)-(c).

To further explore the potential of the S@C composite in resisting crack propagation, more FE simulations are conducted on a series of S@C composite plates with different inclusion radius (R_I) and inter-inclusion spacing (D). The mechanical properties of each phase are kept unchanged, as well as the properties and initial velocity of the projectile. The simulation results including the total crack length, maximum crack radius, and energy absorption by the end of the simulation are plotted in terms of $R_\mathrm{I}/R_\mathrm{p}$ and D/R_p in Fig. 4. It can be seen that crack propagation can be restrained further by reducing the inter-inclusion spacing (D) or enlarging the inclusion radius (R_I). This is because reducing D (with fixed R_I) or increasing R_I (with fixed D) shortens the distance between the impact point and the nearest inclusions, which will effectively enhance the suppression effect of the stiff inclusion on the crack propagation.

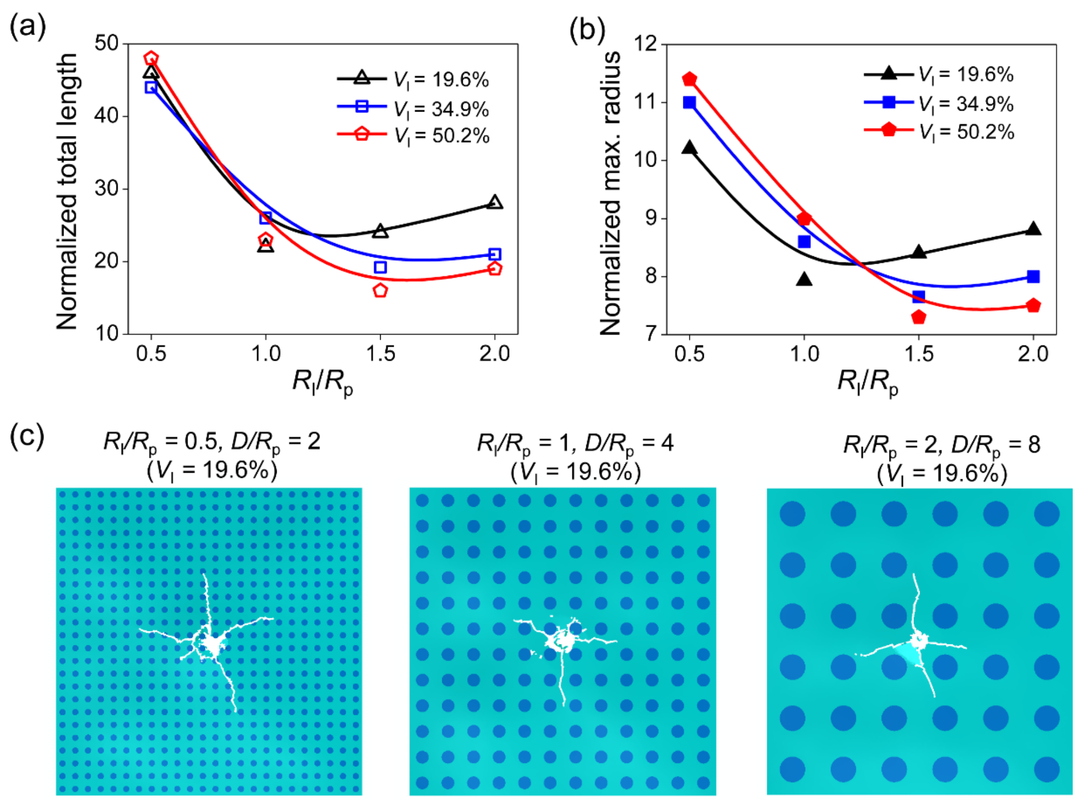

Figure 5. Variations of (a) total length and (b) maximum radius with the normalized radius of inclusions (R_I) for the given volume fraction of the inclusion (V_I). Here, both total length and maximum radius are normalized by the radius of projectile (R_p). (c) The post-impact cracking configuration of the S@C composite plates with the same volume fraction ($V_\mathrm{I} = 19.6\%$) but different $R_\mathrm{I}/R_\mathrm{p}$.

To visualize the effects of R_I and D on cracking, the post-impact configurations are shown in Fig. 4(d) for three selected cases which are marked with a circle, a diamond, and a pentagon symbols in Figs. 4(a-c). Comparison between them reconfirms that larger inclusions (R_I) or shorter inter-inclusion spacing (D) results in higher resistance to ballistic cracking. Given the ratio of R_I/D, namely the volume fraction of the inclusion phase, the variations of the total crack length and maximum crack radius with R_I/R_p are shown in Fig. 5(a) and (b), respectively. It can be seen that the cracking resistance of the S@C composite plates still depends on the size of the stiff inclusion when the volume fraction (V_I) is given. The best performance (minimum cracking) occurs when the inclusion size is around $1{\sim}1.5R_p$. For instance, given volume fraction $V_I = 19.6\%$, the S@C composite plate exhibits the best performance in resisting cracking when the inclusion size is taken as a moderate value of $R_I \cong R_p$, as shown by Fig. 5. The existence of such an optimal inclusion size resulting in the best crack resistance could be interpreted as follows. Given volume fraction (V_I), larger inclusion size implies greater distance between the impact point of the projectile and nearest the stiff inclusions, therefore weaker suppression effect upon the garnered cracks; while if the inclusions are excessively small, the generated dynamic cracks can easily bypass the stiff inclusions by a small deflection when growing, resulting in longer cracks.

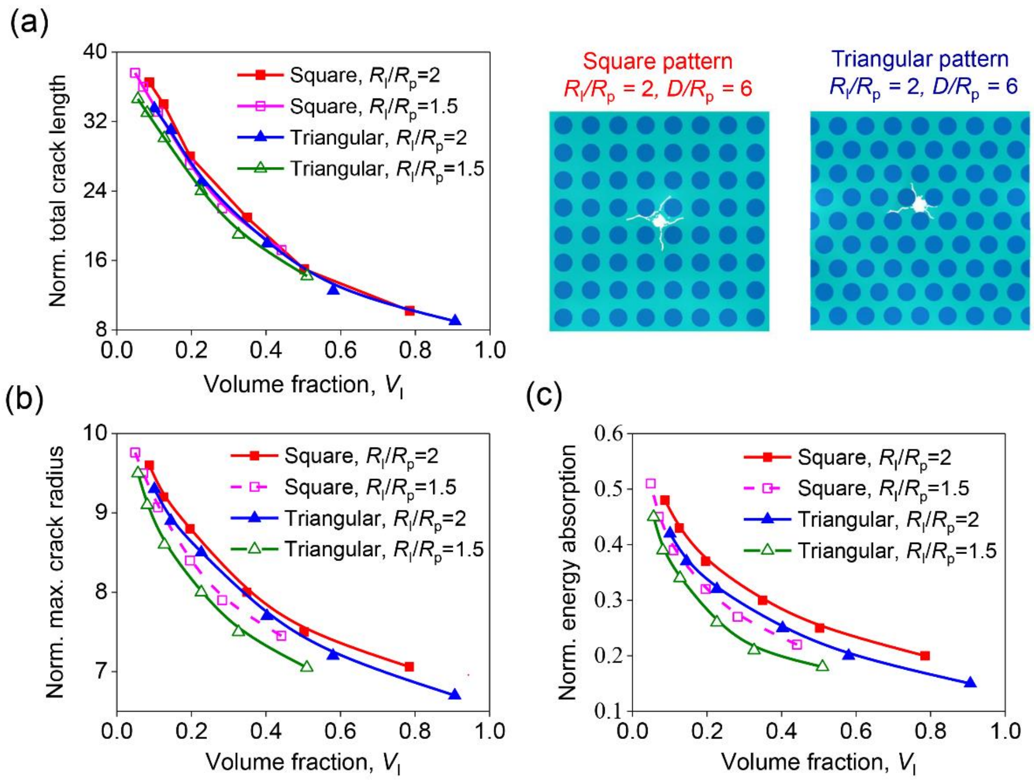

Figure 6. Variations of the normalized (a) total crack length, (b) maximum crack radius,

and (c) energy absorption as functions of volume fraction of stiff inclusion in S@C composite plates with different distribution patterns.

In the above discussion, the stiff inclusions in the S@C composite plates are presumably distributed in a square pattern. To reveal the effect of distribution pattern on the resistance to cracking, we further considered the S@C plates with stiffer inclusions distributed in an equilateral triangular pattern. Figs. 6(a-c) compare the calculated total crack length, maximum crack radius, and energy absorption between the S@C plates with inclusions distributed in different patterns. Given inclusion size, the resistance to ballistic cracking in the S@C plates increases as the volume fraction of inclusions increases. Given both size and volume fraction of inclusion, the triangular pattern results in better resistance to ballistic cracking as compared to the square counterparts. This is mainly due to the smaller distance between the impact point and the nearest stiff inclusions, therefore stronger suppression effect to the cracking, in the triangular pattern as compared to the square pattern with the same inclusion size and volume fraction (Fig. S3).

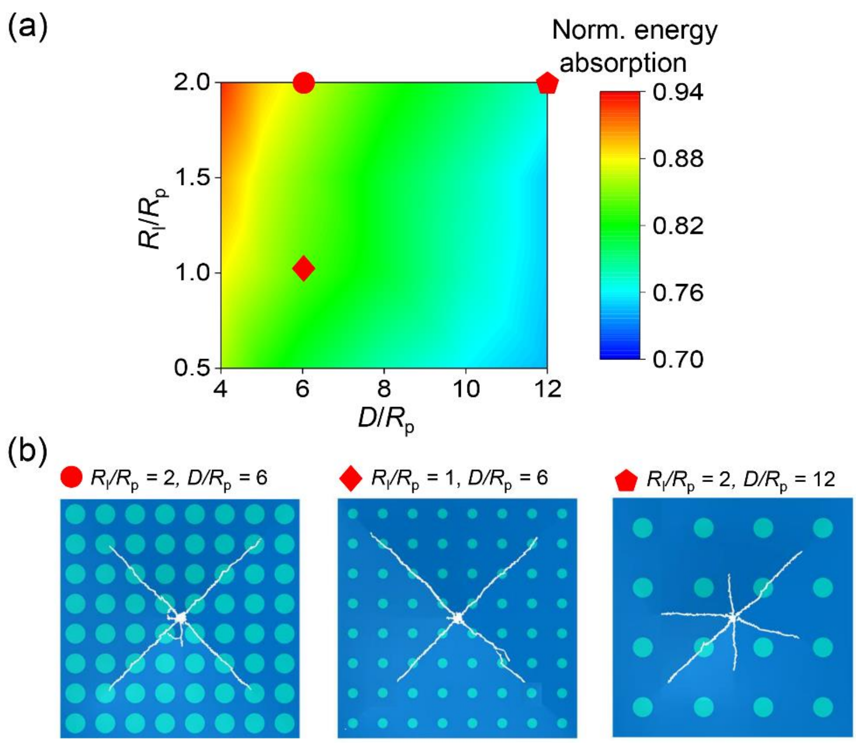

Figure 7. (a) Contour map of energy absorption as a function of inclusion radius (R_I) and inter-inclusion spacing. Here the compliant inclusions are distributed in a pattern. Here energy absorption is normalized by the initial kinetic energy of the projectile. (b)

The cracking configurations of the C@S composite plates after impact by a projectile.

On the other hand, for the complementary C@S composites which exhibit superior energy absorption potential, we investigated the dependence of energy absorption on the size of the compliant inclusions and inter-inclusion spacing, as shown in Fig. 7(a). It can be seen that larger inclusions and smaller inter-inclusion spacing lead to higher energy absorption of C@S composites. The cracking configurations of three selected cases are shown in Fig. 7(b). Similarly, for C@S plates with given volume fraction (V_I), the one with triangular patterned inclusions exhibits relative higher energy absorption in comparison with the one with inclusions in square pattern (Fig. S4).

3.3 Experimental verification

To experimentally verify the effect of stiffness heterogeneity on the resistance to impact cracking, we carried out drop weight tests (Dynatup 9250HV, Instron) on the S@C and C@S plate samples synthesized with polymethyl methacrylate(PMMA) and soda-lime glass. Here, PMMA serves as the compliant (C) phase, while glass serves as the stiff (S) phase. The elastic moduli of PMMA and glass at ambient temperature are 2-3 GPa and ~60 GPa, respectively. Fig. 8(a) shows the schematics of the experimental setup and Figs. 8(b, c) display the images of two types of the composite after the drop weight impact tests. As expected, severe cracking is observed in the C@S (PMMA@Glass) sample, and some cracks initiated from the impact point even penetrate and pass through the PMMA inclusions (Fig. 8(b)). In contrast, in the S@C (Glass@PMMA) sample, fewer and shorter cracks are generated and no clear crack penetration into the glass inclusions is observed (Fig. 8(c)), which is consistent with the prediction of the numerical simulations above. Fig. 8(d) shows the variations of the reaction force exerted on the projectile and the energy absorption (calculated from the loss of kinetic energy of the projectile) with the time. It can be seen that PMMA@Glass plate imposes higher resistant force to the projectile as compared to the Glass@PMMA plate. However, both plates exhibit similar energy absorption even though the cracking in the PMMA@Glass plate is apparently severer than that in the Glass@PMMA plate

(Fig. 8(b, c)). This is basically due to the much higher fracture energies (Γ) of PMMA in comparison to that of the glass, as has been demonstrated by FE simulation (Table S1, Fig. S5).

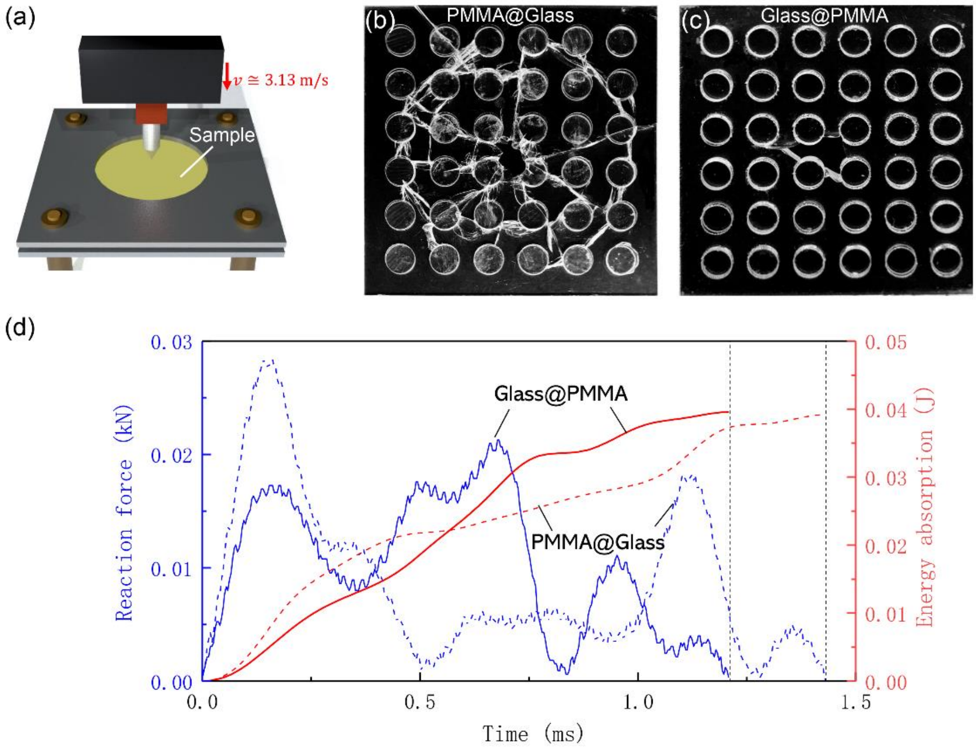

Figure 8. (a) Schematic illustration showing the experiment the drop weight impact test. (b-c) Photos of PMMA@Glass and Glass@PMMA composite plates after drop weight tests. The dimensions of the plates are 100 mm × 100 mm × 2 mm. The diameter of the inclusions is 10 mm, and the inter-inclusion spacing (center-to-center) is 15 mm. To enhance the interfacial strength between the glass and PMMA, the glass surfaces were functionalized with γ-MPS [30]. The drop weight applied was 17.34 kg and the drop height was 0.5 m corresponding to an impact velocity of 3.13 $\mathrm{m \cdot s^{-1}}$. The tup used is a stainless steel cylinder (diameter: 5 mm) with a conical end (included angle ≈85°). (d) Variations of reaction force applied on the projectile (left axial) and energy absorption (right axial) as functions of time. Solid lines and dash lines stand for the drop weight test on Glass@PMMA plate and PMMA@Glass plate, respectively.

4. Discussion and conclusions

In this work, we systematically studied the effects of stiffness heterogeneity on the resistance of composites to impact cracking. It is revealed that impact cracking can be significantly prohibited in S@C composites produced by hybridizing stiff inclusions into a compliant matrix. The performance of S@C composites in prohibiting cracking can be optimized by tuning the size, volume fraction, and distribution pattern of the stiff inclusions. Moreover, the performance of the S@C composites in resisting impact cracking also depends on other practical factors such as the interfacial strength between the S and C phases and the impacting position of the projectile. FE simulations reveal that weak inclusion/matrix bonding would diminish the cracking resistance of the S@C composites especially for the cases with smaller inter-inclusion spacing (Fig. S6); similarly, the cracking resistance of S@C composites will be weakened to some extent if the projectile impacts on the inclusion phase instead (Fig. S7).

On the other hand, for the complementary C@S composites, which are the counterparts produced by hybridizing compliant inclusions into a stiff matrix, are found to facilitate impact cracking and therefore exhibit superior competence in energy absorption. Such distinct mechanical behaviors of these two types of composites in response to the impact loading have also been demonstrated in the experiment. The mechanism behind this phenomenon might be attributed to the inverse proportionality of energy release rate, which can be deemed as the driving force of crack propagation, to the stiffness of material under a given loading or stress intensity factor.

The distinct behaviors of S@C and C@S composites under impact loading endow them with different functionalities in application. For the materials whose structural integrity is crucial, applying the S@C hybridizing scheme could enhance their resistance to cracking. For the energy-absorption materials, which are often used as disposable shields for protection, applying the C@S hybridizing scheme could promote the competence of energy absorption. Moreover, these two types of hybridizing strategies can be used together to exert their synergic effects. For example, we can stack them in tandem to form a double-layer assembly, as shown in Fig. 9. Similar FE simulations under the same ballistic impact as described above show that the cracking configurations of the double-layer assembly depend on the stacking sequence of the plates. If the C@S plate is placed in the front of the S@C plate, the front C@S plate is cracked severely after impact while the rear S@C plate is almost intact (Fig. 9(a)). In contrast, if the S@C plate is placed ahead of the C@S plate, the projectile can penetrate both plates (Fig. 9(b)). A similar phenomenon is also observed in the control double-layer assemblies composed of the monolithic stiff and compliant plates, as shown in Fig. 9(c) and (d). In summary, our work provides a theoretical guideline for harnessing impact cracking by tuning stiffness heterogeneity. This strategy could be applied further to controllably deflect and guide the crack propagation trajectory, and finally constrain the fracture within a limited region [36, 37]. Furthermore, our hybridizing schemes can be applied in combination with other approaches such as applying T-stress [38] to obtain more efficient crack-controlling strategies. These technologies are believed of great value to the design and manufacture of anti-impact materials such as windshields and shields for space stations and satellites [39].

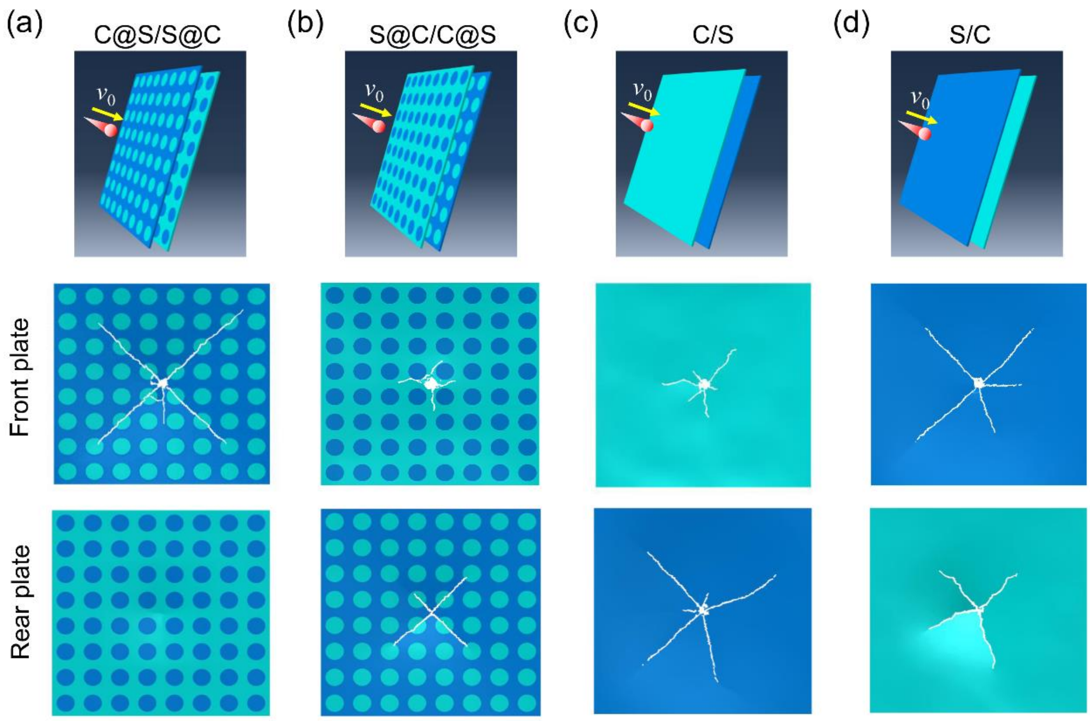

Figure 9. Simulated cracking configurations of double-layer assemblies composed of (a) a C@S plate backed by an S@C composite plate, (b) an S@C plate backed by a C@S plate, (c) a monolithic compliant plate backed by a monolithic stiff plate, (d) a monolithic stiff plate backed by a monolithic compliant plate. In all cases, the two plates are parallel and separated by 1 cm. The radius and spacing between inclusions, if available, are $R_\mathrm{I} = 4$ mm and $D = 12$ mm, respectively.

Declaration of Competing Interest

The authors declare that they have no known competing financial interests or personal relationships that could have appeared to influence the work reported in this paper.

Acknowledgments

This work was supported by the General Research Fund (PolyU 152064/15E) from Hong Kong RGC and the National Natural Science Foundation of China (11772283).

References

[1] W. Sun, F. Lin, X. Hu, Computer-aided design and modeling of composite unit cells, Composites Science and Technology 61(2) (2001) 289-299.

[2] O. Bouaziz, Y. Brechet, J.D. Embury, Heterogeneous and architectured materials: A possible strategy for design of structural materials, Advanced Engineering Materials 10(1-2) (2008) 24-36.

[3] F. Barthelat, Architectured materials in engineering and biology: fabrication, structure, mechanics and performance, International Materials Reviews 60(8) (2015) 413-430.

[4] R. Tao, X. Li, A. Yudhanto, M. Alfano, G. Lubineau, On controlling interfacial heterogeneity to trigger bridging in secondary bonded composite joints: An efficient strategy to introduce crack-arrest features, Composites Science and Technology 188 (2020) 107964.

[5] S. Weiner, H.D. Wagner, The material bone: Structure mechanical function relations, Annual Review of Materials Science 28 (1998) 271-298.

[6] F. Song, A.K. Soh, Y.L. Bai, Structural and mechanical properties of the organic matrix layers of nacre, Biomaterials 24(20) (2003) 3623-3631.

[7] B.H. Ji, H.J. Gao, Mechanical properties of nanostructure of biological materials, Journal of the Mechanics and Physics of Solids 52(9) (2004) 1963-1990.

[8] Z.Q. Liu, M.A. Meyers, Z.F. Zhang, R.O. Ritchie, Functional gradients and heterogeneities in biological materials: Design principles, functions, and bioinspired applications, Progress in Materials Science 88 (2017) 467-498.

[9] T. Liu, K. Huang, L. Li, Z. Gu, X. Liu, X. Peng, T. Kuang, High performance high-density polyethylene/hydroxyapatite nanocomposites for load-bearing bone substitute:

fabrication, in vitro and in vivo biocompatibility evaluation, Composites Science and Technology 175 (2019) 100-110.

[10] J. Li, Q. Zhang, R. Huang, X. Li, H. Gao, Towards understanding the structure-property relationships of heterogeneous-structured materials, Scripta Materialia 186 (2020) 304-311.

[11] H. Yao, Z. Song, Z. Xu, H. Gao, Cracks fail to intensify stress in nacreous composites, Composites Science and Technology 81 (2013) 24-29.

[12] A. Groetsch, P.K. Zysset, P. Varga, A. Pacureanu, F. Peyrin, U. Wolfram, An experimentally informed statistical elasto-plastic mineralised collagen fibre model at the micrometre and nanometre lengthscale, Scientific Reports 11(1) (2021) 15539.

[13] H. Yao, M. Dao, D. Carnelli, K. Tai, C. Ortiz, Size-dependent heterogeneity benefits the mechanical performance of bone, Journal of the Mechanics and Physics of Solids 59(1) (2011) 64-74.

[14] E. Ma, T. Zhu, Towards strength-ductility synergy through the design of heterogeneous nanostructures in metals, Materials Today 20(6) (2017) 323-331.

[15] T.S. Cook, F. Erdogan, Stresses in bonded materials with a crack perpendicular to the interface, International Journal of Engineering Science 10(8) (1972) 677-697.

[16] F. Erdogan, G.D. Gupta, M. Ratwani, Interaction between a circular inclusion and an arbitrarily oriented crack, Journal of Applied Mechanics 41(4) (1974) 1287–1297.

[17] M.Y. He, J.W. Hutchinson, Crack deflection at an interface between dissimilar elastic-materials, International Journal of Solids and Structures 25(9) (1989) 1053-1067.

[18] O. Tamate, The effect of a circular inclusion on the stresses around a line crack in a sheet under tension, International Journal of Fracture Mechanics 4(3) (1968) 257-266.

[19] C. Atkinson, The interaction between a crack and an inclusion, International Journal of Engineering Science 10(2) (1972) 127-136.

[20] A. Boulenouar, N. Benseddiq, M. Mazari, Strain energy density prediction of crack propagation for 2D linear elastic materials, Theoretical and Applied Fracture Mechanics 67-68 (2013) 29-37.

[21] C. Wang, W. Libardi, J.B. Baldo, Analysis of crack extension paths and toughening in a two phase brittle particulate composite by the boundary element method, International Journal of Fracture 94(2) (1998) 177-188.

[22] S. Jiang, D.U. C., G.U. C., X. Chen, XFEM analysis of the effects of voids, inclusions and other cracks on the dynamic stress intensity factor of a major crack, Fatigue & Fracture of Engineering Materials & Structures 37(8) (2014) 866-882.

[23] S. Jiang, C. Du, Study on dynamic interaction between crack and inclusion or void by using XFEM, Structural Engineering & Mechanics 63(3) (2017) 329-345.

[24] K.B. Tran, T.T. Truong, An investigation into the effects of holes, inclusion on crack growth in composite material under dynamic load by extended twice - interpolation finite element method, Proceedings of International Symposium on Applied Science 2019 3 (2020) 1-10.

[25] W. Limtrakarn, Stress intensity factor KI and crack–hard inclusion interaction study of a single edge cracked plate by adaptive remeshing and photoelasticity, Applied Science and Engineering Progress 13(4) (2020) 336-345.

[26] R.S. Yang, C.X. Ding, L.Y. Yang, P. Xu, C. Chen, Hole defects affect the dynamic fracture behavior of nearby running cracks, Shock and Vibration 2018 (2018) 5894356.

[27] X. Zeng, Y. Wei, Crack deflection in brittle media with heterogeneous interfaces and its application in shale fracking, Journal of the Mechanics and Physics of Solids 101 (2017) 235-249.

[28] Z.-E. Liu, Y. Wei, An analytical solution to the stress fields of kinked cracks, Journal of the Mechanics and Physics of Solids 156 (2021) 104619.

[29] M. Lebihain, J.-B. Leblond, L. Ponson, Effective toughness of periodic heterogeneous materials: the effect of out-of-plane excursions of cracks, Journal of the Mechanics and Physics of Solids 137 (2020) 103876.

[30] A. Amini, A. Khavari, F. Barthelat, A.J. Ehrlicher, Centrifugation and index matching yield a strong and transparent bioinspired nacreous composite, Science 373(6560) (2021) 1229-1234.

[31] M. Kamble, A.S. Lakhnot, N. Koratkar, C.R. Picu, Heterogeneity-induced mesoscale toughening in polymer nanocomposites, Materialia 11 (2020) 100673.

[32] Z. Jia, L.F. Wang, 3D printing of biomimetic composites with improved fracture toughness, Acta Materialia 173 (2019) 61-73.

[33] T.L. Anderson, Fracture mechanics: fundamentals and applications, CRC Press1991.

[34] Y.E. Murakami, H. Tsuru, The stress intensity factors handbook, Pergamon press, Oxford, 1987.

[35] A. Hillerborg, M. Modéer, P.-E. Petersson, Analysis of crack formation and crack growth in concrete by means of fracture mechanics and finite elements, Cement and Concrete Research 6(6) (1976) 773-782.

[36] C. He, Z. Xie, Z. Guo, H. Yao, Fracture-mode map of brittle coatings: Theoretical

development and experimental verification, Journal of the Mechanics and Physics of Solids 83 (2015) 19-35.

[37] J.-F. Fuentealba, E. Hamm, B. Roman, Intertwined multiple spiral fracture in perforated sheets, Physical Review Letters 116(16) (2016) 165501.

[38] K. Guo, B. Ni, H. Gao, Tuning crack-inclusion interaction with an applied T-stress, International Journal of Fracture 222(1-2) (2020) 13-23.

[39] E. Grossman, I. Gouzman, R. Verker, Debris/micrometeoroid impacts and synergistic effects on spacecraft materials, MRS Bulletin 35 (2010) 41-47.